NANO LETTERS

Letter

pubs.acs.org/NanoLett

Topological Dynamics in Supramolecular Rotors

Carlos-Andres Palma,*[,†] Jonas Björk,[‡] Francesco Rao,[§] Dirk Kühne,[†] Florian Klappenberger,[†] and Johannes V. Barth*[,†]

[†]Physik-Department E20, Technische Universität München, D-85748 Garching, Germany

[‡]Department of Physics, Chemistry, and Biology (IFM), Linköping University, 58183 Linköping, Sweden

[§]Freiburg Institute for Advanced Studies (FRIAS), Albert-Ludwigs-Universität Freiburg, 79104 Freiburg, Germany

Supporting Information

ABSTRACT: Artificial molecular switches, rotors, and machines are set to establish design rules and applications beyond their biological counterparts. Herein we exemplify the role of noncovalent interactions and transient rearrangements in the complex behavior of supramolecular rotors caged in a 2D metal−organic coordination network. Combined scanning tunneling microscopy experiments and molecular dynamics modeling of a supramolecular rotor with respective rotation rates matching with 0.2 kcal mol^{-1} (9 meV) precision, identify key steps in collective rotation events and reconfigurations. We notably reveal that stereoisomerization of the chiral trimeric units entails topological isomerization whereas rotation occurs in a topology conserving, two-step asynchronous process. In supramolecular constructs, distinct displacements of subunits occur inducing a markedly lower rotation barrier as compared to synchronous mechanisms of rigid rotors. Moreover, the chemical environment can be instructed to control the system dynamics. Our observations allow for a definition of mechanical cooperativity based on a significant reduction of free energy barriers in supramolecules compared to rigid molecules.

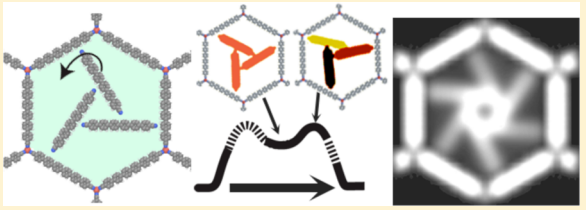

KEYWORDS: *Molecular dynamics, STM, metal−organic networks, nanopore, rotation, chirality, molecular engineering, supramolecular dynamer*

Atomic-level description, and ultimately prediction, of molecular systems with spatiotemporal resolution of the microscopic processes is a crucial objective of physical chemistry and nanoscale science. All-atom mechanistic modeling stands as a universal method toward this goal, which has already accomplished the monumental tasks of de novo protein design,[1] elucidation of mega-Dalton protein structure,[2] and has recently been recognized[3] to having revolutionized the multiscale description of complex biological systems. Indeed systems' biomolecular chemistry enjoys a privileged status where intricate mechanisms of molecular machinery have been portrayed, albeit experimental evidence with high spatiotemporal resolution remains challenging. For instance, mechanisms in protein chemomechanics[4] have been progressively refined to include ion-channel gating via twisting,[5] synchronous rotation around the axis of the ATPase[6] and asynchronous stepping of dynein.[7] Conversely, although man-made fabrication of molecular materials and machines is expected to grow boundlessly beyond biology,[8] complex all-atom modeling in the field is just being developed.[9−11] One specific topic in artificial molecular machines that has attracted attention from fundamental physics,[12] chemistry[13−16] and nanoscience[17−25] is mechanical rotation. Either unidirectional processes have been described driven by external stimuli[20−23] or randomly rotating systems operating at thermal equilibrium.[17,19,24] Strategies for controlling the pertaining intricate mechanisms have been anchoring of rotatable molecular units to surfaces[22,23,25] or their incorporation into larger molecular architectures.[21] For such systems, while the ground state[20,25] and ensemble thermodynamics[16] were described in great detail, the kinetics and mechanistic pathways have been elusive from the experimental point of view because of inherent short-lived intermediate configurations or transition states, which are associated in the present work with "the full family of configurations through which a reaction evolves".[26] An appealing approach to study molecular rotation consists of confinement[19] in two-dimensional nanopores for which a well-defined environment provided by 2D metal−organic networks[27] (MONs) assembled on a Ag(111) substrate can be employed. Using this strategy, we have reported on a dynamic supramolecule (a dynamer) that undergoes confined rotation in a nanoscopic pore.[24]

Here, we perform a combined investigation with scanning tunneling microscopy (STM) and molecular dynamics (MD) modeling, allowing for a full thermodynamic and kinetic description of supramolecular dynamers. Aided by a recent high-quality parametrization[28] of the pore and of the intermolecular interactions, the simulations reproduce experimentally observed thermodynamics of monomeric, dimeric, and trimeric supramolecular system with exquisite atomic

Received: April 16, 2014
Revised: July 12, 2014
Published: July 31, 2014

   dx.doi.org/10.1021/nl5014162 | *Nano Lett.* 2014, 14, 4461−4468

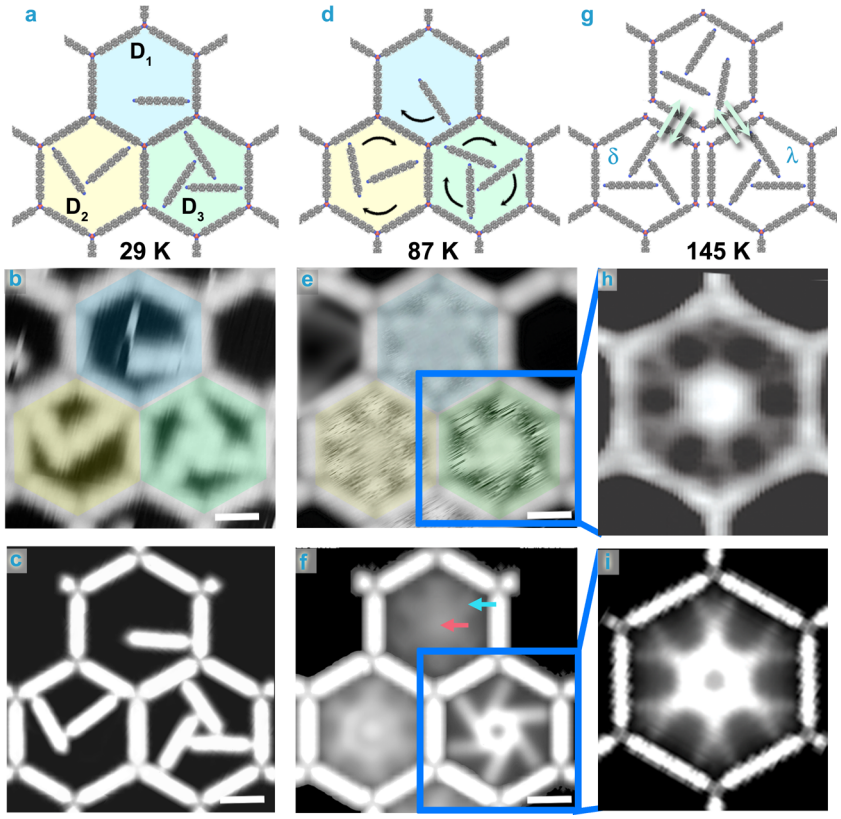

Figure 1. Appearance of dynamers caged in metal−organic network pores. (a,b) Scheme for the static state of the molecules and STM image at 29 K. (c) Rendering of the molecules in the pore by mapping their occupation. (d) Scheme with multiple intrapore configurations at higher temperatures. (e) STM at 87 K showing the time-average pattern (TAP) of D_1, D_2, and D_3 (blue, yellow, and green hexagons, respectively). (f) Corresponding TAPs from microseconds-long MD simulations. Each independent simulation is placed as in the experiment in (e). Arrows indicate the main differences compared to experimental data in (e). (g) Scheme illustrating chiral inversion of a D_3 propeller structure; different enantiomers are labeled δ and λ. (h) The STM TAP at 145 K of D_3 shows a 12-branched star resulting from the superposition of 2 rotating propellers with opposite handedness. (i) TAP from 0.5 μs-long MD at 450 K. STM parameters U_T = 2.0 V, I_T = 0.1 nA. Sexiphenyl dicarbonitrile *N*-to-*N* length is 30 Å and scale bars are 20 Å. Rendering of the silver substrate is omitted in the models for clarity.

detail. Low-temperature intermediate structures found in the experiment are also atomically resolved and the employed classical thermostats reproduce with high fidelity the experimentally extrapolated rotation rates of the trimeric supramolecular dynamer. Using these quantitative indicators, we borrow concepts from mathematics and coordination chemistry[29] to describe topological conserving and nonconserving mechanisms in supramolecular rotation and stereoisomerism. Our studies reveal energy optimization strategies in the mechanics of man-made elements of supramolecular machinery, therewith unraveling new concepts in mechanical cooperativity.

After fabricating a highly regular MON,[27] additional evaporation of molecules onto the MON architecture results in the confinement of monomers (D_1) and dimeric (D_2) or trimeric dynamers (D_3) in different pores as schematically depicted in Figure 1a. Notably, a three-membered sexiphenyl dicarbonitrile[24,30] dynamer (D_3) is held together in a propeller shape via three internal noncovalent bonds and acts as a rotator. The rotator interacts via three further noncovalent bonds with the MON's frame, which acts as the stator. Carefully adjusting the surface concentration makes it possible to simultaneously visualize MON pores occupied with different species by STM. Figure 1a,b depict the schematics and STM data of the respective ground-state configurations at 29 K. Figure 1c shows a rendering constructed from an all-atom model by projecting each atom into a 3D pixel (see Supporting Information Experimental Procedures). Increasing the temperature on such systems provokes an articulated molecular motion that can be understood as molecules rotating and translating inside the pore as illustrated by the models in Figure 1d. With the limited time resolution of the STM, this motion leads to distinct time-averaged patterns (TAP) at 86 K in Figure 1e. Figure 1f demonstrates how such TAPs can be reproduced from microseconds-long MD simulations, where the occupation of each pixel is averaged among the number of frames rendered (typically 2×10^4). Classical MD simulations were performed through the Langevin thermostat, in conjunction with a custom-made electrostatic parametrization[28] and the c22 CHARMM force field (see Supporting Information Experimental Procedures). Symmetry and occupation probabilities of the simulated and experimental images, in Figure 1e,f, are in good agreement. Notice how the simulated TAPs are a smooth average, whereas the experimental TAPs D_2 and D_3 display frizzly features. In STM, such streaking occurs when the rates (Γ) of scanning and molecular displacements come close, whereby the "streakiness" is smeared out over a characteristic pattern for very rapid motions.[24] The STM data thus indicates that Γ [D_1] > Γ [D_2] > Γ [D_3] at the corresponding temperature. Two main differences between experimental and simulated TAPs can be pinpointed. First, a common discrepancy in all simulated images is the low probability

dx.doi.org/10.1021/nl5014162 | *Nano Lett.* 2014, 14, 4461−4468

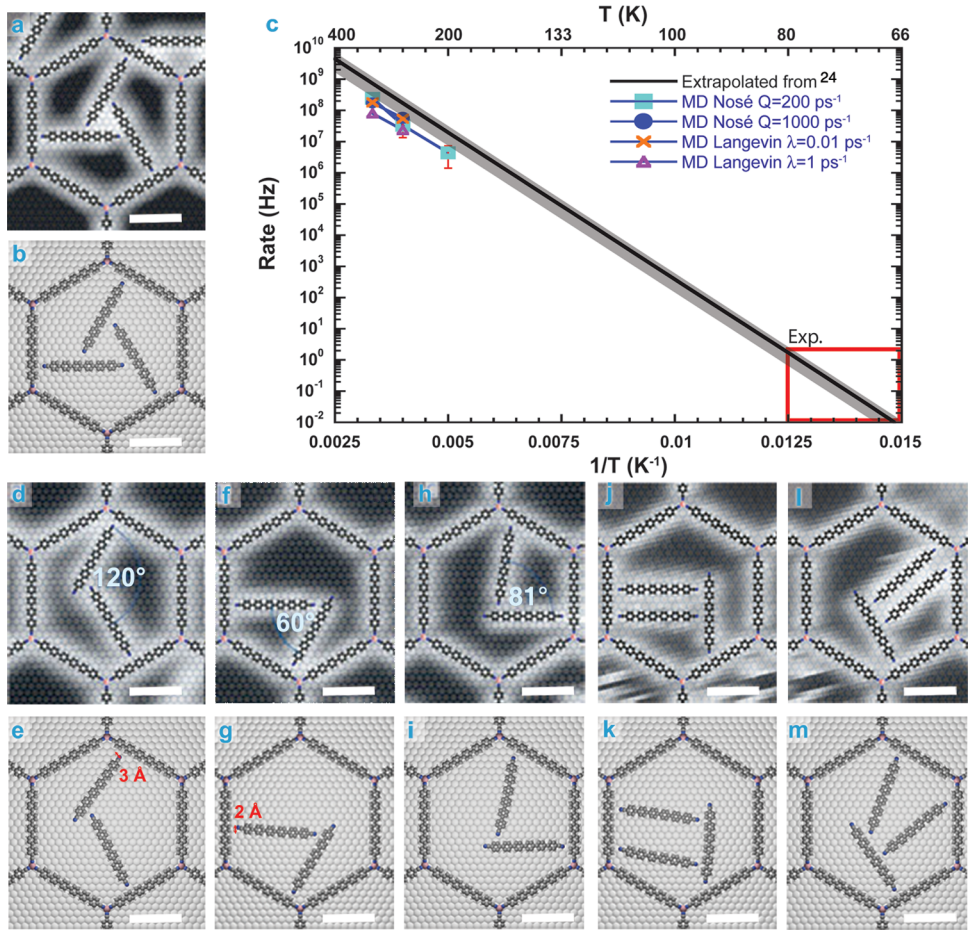

Figure 2. Kinetic analysis of D_2 and D_3 caged dynamers. (a,b) STM image of the D_3 molecular rotator ground state and corresponding MD simulations. (c) Rotation rate plot from MD simulations at 250, 300, and 350 K using different friction coefficients Q and λ, for the Nosé and Langevin thermostats, respectively (blue lines). The extrapolated rate[23] from the experiments carried out between 65 and 79 K (red box) is in black with uncertainty shown in gray. (d,f,h) STM images at 24−26 K of D_2 featuring opening angles of 120, 60, and 81°. (e,g,i) MD snapshots at 250 K showing the low-temperature configurations in (d,f,h). (j,l) STM images at 62 K of transient "Π" structures for D_3. (k,m) Snapshots of "Π" configurations appearing during MD simulations at 450 K. STM parameters U_T = 2.0 V, I_T = 0.1 nA. Scale bars are 20 Å.

near the corners of the pore (blue arrow, Figure 1f) compared to experiment. Second, for D_1 and D_2 rapidly moving, the center of the pore appears brighter in the simulations (Figure 1f magenta arrow). These differences are ascribed to the higher temperatures required for the MD simulations (see Supporting Information Experimental Procedures). Additionally, these contrast differences include a contribution from the colder temperature near the pore's frames, caused by freezing the frame's atoms (see Supporting Information Experimental Procedures and ref 28 for details).

Importantly, a second type of TAP for the D_3 dynamer different from the propeller shape in Figure 1e,f is observed by increasing the temperature to 145 K (Figure 1h). This 12-branched TAP occurs for the D_3 dynamer system and has been assigned[24] to a convolution of propeller shapes with opposite handedness (δ and λ, Figure 1g). In other words, there is a dynamic stereoisomerization of the caged D_3. In the simulated TAP, such pattern is also reproduced at much higher temperatures of 450 K (Figure 1i), albeit with a restraining vertical potential in order to prevent the molecules escaping from the pore at such elevated temperatures (see Supporting Information Experimental Procedures).

Our simulation method allows for detailed thermodynamic reproduction of the long-lived metastable states dominating the experimental TAPs. However, intermediate configurations must be carefully replicated for an asserted disentanglement of single-molecular motion. For the D_3 species, the experimental and simulated ground state is elucidated with great level of atomic detail in Figure 2a,b. In such configuration resembling a propeller, the dynamer topology is defined by each molecule featuring only one nitrogen−phenylene interaction with the side of a neighbor, for a total of three internal noncovalent bonds, enclosing an area in the center of the pore. We have previously classified such in-plane noncovalent interactions between nitrogen and arene rings as proton acceptor-ring (PAR) interactions.[31] Starting at 150 K in the microsecond simulation time scale, molecular rotation can already be detected. From 200 to 300 K, simulated molecular rotation events (60° turns) were statistically analyzed and the respective rates plotted in Figure 2c. When the experimental rotation rates[19] are extrapolated to these temperatures, there is a good agreement with the simulations, being $(5.6 \pm 2.6) \times 10^7$ Hz for a Langevin low-friction simulation and $(1.8 \pm 1.1) \times 10^8$ Hz for the experimental extrapolated rate at 250 K. Considering an experimental pre-exponential factor[23] of 1.3 ($\pm$0.8) $\times 10^{12}$ Hz, free energy barriers from simulation and experiment can be computed as 0.195 eV (4.5 kcal mol^{-1}) and 0.186 eV (4.3 kcal mol^{-1}), respectively. Although the barrier difference of 0.2 kcal

dx.doi.org/10.1021/nl5014162 | Nano Lett. 2014, 14, 4461−4468

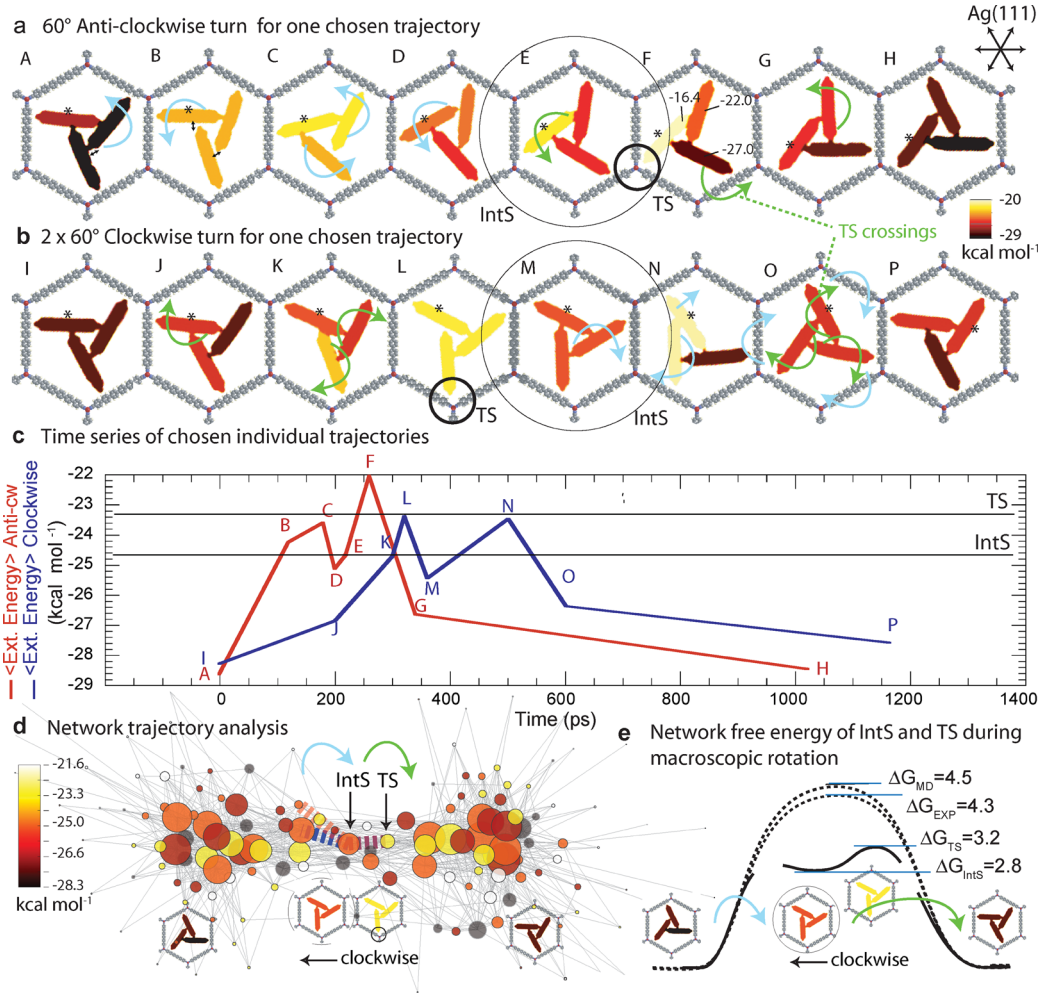

Figure 3. Mechanisms of supramolecular rotation. (a,b) Rendered snapshots of a single counterclockwise and two clockwise rotations from 250 K MD simulations. Green/blue arrows indicate the next movement in the series. An asterisk is used to identify the same molecule and guide the eye during rotation. The intermediate state (IntS) is circled; for one selected transition state (TS) one carbonitrile points toward the cobalt coordination note (small black circle). Except for structure F, colors are scaled to energy (see inset). (c) MD time series of the average energy per molecule during anticlockwise (red) and clockwise (blue) rotations with key configurations highlighted. (d) Network analysis of 10^4 snapshots. The node's color corresponds to the energy and the size is proportional to each node's degree (i.e., visiting probability). Trajectories from D to F and from L to N in (c) are indicated in red and blue dashed lines accordingly. (e) Qualitative rotation free energies extracted from the network analysis for IntS and selected TS states. Experimental (ΔG_{EXP}) and simulated (ΔG_{MD}) rotation free energies, obtained from the Arrhenius representation in Figure 2b, are also shown (T = 250 K).

mol^{-1} is within the experimental error, precision can be improved by parameter refinement or enhanced thermalization of the pore (due to the colder temperature of the pore's rim in the simulations, see Supporting Information Experimental Procedures). When performing simulations thermalizing the network's rim hydrogens, however, the rotation rate was not significantly affected, leaving room for further thermalization improvement. It is worth noting that above 300 K, a transition from flat to edge-on adsorption geometry occurs on the simulation time scales with our parametrization. This is expected because hopping of molecules between pores is observed in experiments already setting in at temperatures exceeding 145 K. Thus, 2D harmonic, vertically restraining potentials are needed in order to avoid trapping of unphysical states at temperatures higher than 300 K. Because of this, in what follows the free energy analysis is performed exclusively at 250 K: a temperature high enough for rotation and low enough to avoid desorption on the microsecond time scale.

It is important to relate states found in simulations to those observed in experiments. At cryogenic conditions, however, only one state, the ground state in Figure 2a, is observed for the D_3 molecular rotator. A better assessment of the supramolecular dynamer configurations in the 20−30 K range can be achieved for the D_2 dynamer, where the intermediate structures shown in Figures 2d,f,h could be identified in the STM data. The corresponding simulated structures correlate nicely with the experimental ones showing maximum atom−atom distance differences of 3 Å (cf. Figure 2e−i differences have been labeled in red). Upon increasing the experimental measurement temperature to 62 K, two transient structures for the D_3 molecular rotor could be observed (Figure 2j,l). These "Π" configurations differ from the propeller arrangement in that they present one noncovalent bond less between the constituents and two CN moieties attached to one molecule's phenylene backbone. Thus, a new topology without any enclosed area between the dynamers is formed. "Π" configurations also appear in MD simulations (Figure 2k,m)

dx.doi.org/10.1021/nl5014162 | Nano Lett. 2014, 14, 4461−4468

and feature the same topology as in the experiment. However, a broader geometry appears, caused by the limitation of the force fields in reproducing a stable parallel dimer configuration. In other words, without appreciable short-range vdW interactions and/or screening of the 24 electro-positive hydrogens less than 5 Å apart an in-plane parallel dimer is highly repulsive. Despite this drawback, the simulations are able to reproduce a wider "Π" analogue, which plays a central role in the stereo-isomerization pathways of the D_3 dynamer as described below.

Next we consider the mechanism of rotation for the D_3 supramolecular dynamer at the MD simulation temperature of 250 K. First, we randomly choose single trajectories and extract the external energy of each molecule every 20 ps. The external energy is defined as the energy of the molecule in the pore, minus that of the isolated molecule alone (frozen in the geometry it has in the pore). The ground-state external energy of the D_1 monomer at 250 K is close to −0.75 eV (−17.3 kcal mol^{-1}, see note in ref 32). In our model, this external energy has an electrostatic contribution of 0.36 eV (−8.3 kcal mol^{-1}, see note in ref 33) that can be understood as the one PAR interaction plus the substrate's electrostatic interaction. For a D_3 dynamer in the ground state (in frame A, Figure 3a) the average external energy per molecule increases to −1.21 eV (−27.9 kcal mol^{-1}) of which 2/3 are due to electrostatics. Because each molecule in the D_3 dynamer propeller configuration is interacting with two molecules, the difference between the D_1 and D_3 ground-state energies corresponds to approximately two internal PAR interactions (i.e., within the dynamer excluding the rim). The last statement indicates that each internal PAR interaction amounts to −0.23 eV (−5.2 kcal mol^{-1}), which is in agreement with quantum chemical calculations of lateral dicarbonitrile oligophenylene PAR interactions with an energy of −0.22 eV[34] (−5.1 kcal mol^{-1}, see note in ref 35). These insights allow for the analysis of interactions for individual molecules with the respective surroundings during the D_3 dynamer rotation in the pore.

With this in mind, we map and analyze rotation events for the D_3 propeller system (Figure 3a,b) by choosing a structure subset of interest along individual time series paths (Figure 3c, see Supporting Information Figure S1 for the full trajectory). In the first step toward a 60° anticlockwise rotation, a single molecule turns only a few degrees (circular arrows in A, Figure 3a). This movement is large enough to partially weaken two inner PAR interactions, from a CN, nearest hydrogen distance of 2.7 Å to one of 4.3 Å (small black arrows in A,B Figure 3a), effectively increasing the external energy by an average per molecule of 4 kcal mol^{-1} (compare Figure 3c point A,B). This state is further destabilized by continuing an anticlockwise movement as in C, Figure 3a. Once the barriers from A to C are overcome, the propeller restructures transiently (D, Figure 3a) into the long-lived intermediate state E (belonging to the IntS family). Note that this intermediate state has effectively the same symmetry as the ground state A but does not align with the Ag(111) high-symmetry directions (cf. Figure S3 in ref 24). As a consequence, the energy is expected to be slightly higher for E. By breaking a rim PAR interaction in E, the dynamer attains the important state F in Figure 3a. Structure F is considered as belonging to a family of configurations representative of a selected transition state (TS), characterized by having a carbonitrile directly pointing toward the cobalt coordination node. Consequently there are at least two additional symmetry elements (120 and 240°) for every identified selected configuration of the TS family. The ab initio electrostatic potential, employed to parameterize our force field,[28] indicates that the coordination sphere of the cobalt is strongly negative. This electrostatic landscape is reproduced in our force field by a negatively charged cobalt atom (cf. Figure 3 in ref 28). Therefore, the nitrogen−cobalt interaction is highly unfavorable, justifying the initial choice of states belonging to a TS family. Subsequently, in order for the ground state to perform a full 60° rotation, the selected TS must be crossed at least two additional times (Figure 3a, green arrows): one additional time going to state G, and another completing the full rotation event to state H. Note that at 250 K these steps are asynchronous, for example, during 0.6 ns state G crosses the selected TS back and forth more than three times, without preferential order, before finally arriving to state H. Altogether, the energetics of the supramolecular rotor depend on the interplay between (1) adsorbate−adsorbate interactions, (2) adsorbate−pore interactions, (3) adsorbate substrate registry, and (4) adsorption height.

The previously identified pathway to reach the selected TS becomes the first important step during a 60° clockwise rotation from I to O in Figure 3b; note that the pathway M−K is identical to the E−G, albeit showing different L and F structures. The L structure corresponds to the prevalent TS in the E−G pathway we pointed out previously, where one molecule points toward the cobalt atom. Halfway through the 60° clockwise turn, the rotator recovers again an intermediate exactly equal to E, this time, dubbed structure M. This marks again an element of the IntS family, that is, a position of 40° during the 60° rotation. The IntS state is especially important because, besides the ground state, it is the only symmetric intermediate during rotation. In other words, only the ground state and the IntS state appear to behave as one symmetry-defined supramolecule. All other states belonging to the dynamer undergo distortions to cross barriers atemporally, via structures differing from the ground state or IntS and thus, the rotational dynamics are asynchronous in the movement of the supramolecule's constituents. Importantly, such asymmetric structures do conserve the supramolecular topology characteristic of the ground state and the IntS, that is, they are homeomorphic with each other along the reaction pathway. Broadly speaking, as long as the propeller is considered as intermolecularly connected, it will feature an enclosed area and share topology with a torus (Euler characteristic of $X = 0$). It is worth mentioning that in contrast to our spatiotemporal MD model, the experiments provided no evidence for assembly deassembly processes, whence the rotation was interpreted as a concerted mechanism.[24] Concerted motions should not involve intermediate states,[36] a concept put into question by time-resolved experiments, where intermediate states can be identified. Therefore, the mentioned classifications based on topological (homeo- versus heteromorphic) and temporal properties (synchronous versus asynchronous) are expected to enrich the description of supramolecular dynamics beyond the concerted reaction concept.

The above analysis of individual trajectories points out that the rotation is a two-step process. First, a variety of pathways allow the rotor to move into the IntS structure (cyan arrows in Figure 3). Second, the rotator surpasses the TS configurations at least three times to complete a 60° rotation (green arrows in Figure 3). To give statistical evidence of this observation, network analysis[37,38] was conducted on 2×10^4 configurations by grouping them into external energy, spatial configuration, and rotation capacity and then positioning the groups (nodes)

dx.doi.org/10.1021/nl5014162 | Nano Lett. 2014, 14, 4461−4468

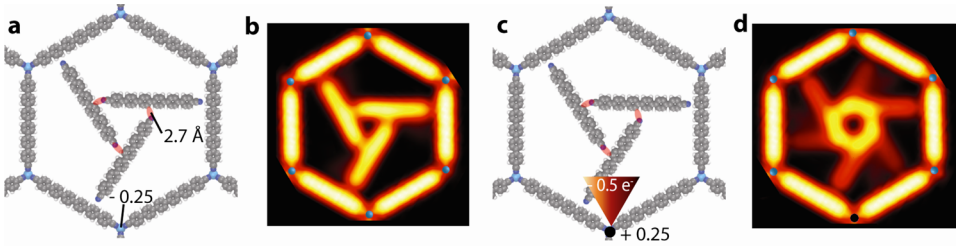

Figure 4. In silico electronic manipulation of a rigid rotor. (a) The D_3 dynamer is constrained by artificial 2.7 Å N−H bonds (in red) transforming it into a rigid rotor. (b) The TAP of 0.75 μs-long (4×10^4 frames) MD simulations at 350 K shows no rotation events in the rigid rotor. (c) One cobalt atom representing the coordination sphere in the employed model (in black) is modified from −0.25 to 0.25 local charge state in a thought experiment. (d) The TAP of 0.75 μs-long MD simulations at 350 K shows that one positively charged cobalt coordination sphere in the rim is enough to switch molecular rotation back on.

with a Fruchterman−Reingold force-directed algorithm.[39] The rotation capacity of each structure is defined as zero if none of its $n < 5$ future positions is engaged in 60° directional rotation and two otherwise (see Supporting Information Figure S2). With this definition, the network in Figure 3d with node size reflecting the connectivity degree and color indicating the average external energy per molecule naturally summarizes the previous observations. The IntS intermediate state is shown connecting the two valleys of 60° rotational symmetry each. The clustered TS state is now the shortest path between one valley and the IntS state. The population-based free energies, deduced from the network analysis (see Supporting Information Figure S1), of the clustered TS and IntS states are illustrated in Figure 3e. The figure depicts the rotation process again as a two-step process where the dynamer moves asynchronously to an intermediate IntS and finally crosses the selected TS state toward a full 60° rotation (cyan and green arrows, respectively). Importantly, transition free energies can be obtained through the network analysis, albeit with an error proportional to the clustering algorithm energy resolution, here 0.07 eV per molecule (1.7 kcal mol^{-1}, see Supporting Information Figure S2). Such broad clustering is necessary because of the limited time resolution employed (20 ps). Quantitative clustering analysis should make use of time resolutions much below the lifetime of the TS (1 ps), which translates to analyses of $>10^6$ snapshots, currently unreachable by our graphical method. Thus, by taking the logarithm of the population ratios in the selected TS and IntS states (see Supporting Information Figure S2) times the temperature (250 K) and gas constant, the network analysis provides an estimate for a qualitative TS barrier of 3.2 kcal mol^{-1} and an IntS of 2.8 kcal mol^{-1}. Despite the aforementioned qualitative estimations, the energy barrier of rotation from the network analysis is underestimated by only 1.1 kcal mol^{-1} compared to the experimental rotation barrier of 4.3 kcal mol^{-1} (obtained from the previous analysis of Figure 2c). Note that Figure 3e considers only the free energies of the two majority states IntS and TS during rotation and does not imply that the overall free energy barrier between 0 and 60° rotation is asymmetric.

The trajectory and network analysis suggests that for a fully synchronous rotation (i.e., arising from a rigid propeller instead of a supramolecule) the new rate-limiting transition barrier should have at least three times the energy of the previously described TS barrier. This energy would be close to 9.6 kcal mol^{-1} because at any given time the rotor's nitrogens would be required to point toward the cobalt atoms simultaneously and therefore overcome three one-molecule 3.2 kcal mol^{-1} transient states simultaneously. To prove this, simulations were carried out with a rigid propeller. First, the dynamer was constrained with harmonic bonds between one molecule's nitrogen and an adjacent molecule's phenylene hydrogen (Figure 4a, red ellipses). This time, no rotation events were detected in 0.75 μs-long simulations at temperatures of 350 K (TAP in Figure 4b). To turn back on rotation in the rigid propeller in the simulation time scale, an in silico experiment can be carried out. As previously discussed, an energy barrier intervenes when the partially negative nitrogen atom points toward the partially negative cobalt−nitrogen coordination sphere (parametrized as a negative cobalt atom). By an ad hoc increase of the positive charge at one out of the six cobalt atoms, the rotation barrier diminishes (Figure 4c). Such a local modification of the coordination node can be achieved, for instance, by attaching an axial ligand at the coordinatively unsaturated metal center or possibly by using the STM tip to transiently alter the charge distribution in the metal−organic architecture. A total of half an electron is removed from the cobalt force field simulating such a transient charging. Figure 4d accordingly reveals a TAP after 0.75 μs of the modified cage. As expected, a total of four rotation events now occur under the same conditions (Figure 4d) at a rate of $\sim 5.3 \times 10^6$ Hz. This frequency is approximately 2 orders of magnitude (10^2) lower than obtained for the supramolecular rotator at the same temperature (Figure 2c, $\sim 10^8$ Hz at 350 K). Consequently, the barrier of rotation of a (rigid) covalent rotor in a pore with positively charged coordination node increases at least by an additional RT $\ln(10^2)$ to ca. 7.5 kcal mol^{-1}.

Analogous to chemical cooperativity (where a process' free energy is higher for one molecule than for many), our observations point toward the importance of mechanical cooperativity (where a process' free energy for a rigid covalent molecule exceeds that of a flexible or supramolecule) in molecular rotation. This is in line with asynchronous processes being favored by entropy, because of the multiple path permutations or steps[7] a molecular motor may choose toward movement.

Finally, it is of importance to differentiate between asynchronous, homeomorphic processes (D_3 propeller rotator in Figure 1d−f) and asynchronous nontopology conserving, that is, heteromorphic processes like those interfering during stereoisomerization in Figure 1h,i (cf. Table 1). To this end, we analyze an individual randomly chosen MD trajectory where stereoisomerization is observed (Figure 5). Now, the supramolecule is shown breaking the propeller topology by completely detaching one molecule (C in Figure 5). The last step entails the formation of the transient "Π" structure (D in Figure 5, belonging to a different topology without an enclosed

dx.doi.org/10.1021/nl5014162 | Nano Lett. 2014, 14, 4461−4468

Table 1. Classification of Two-Dimensional Reaction Pathways According to Topology Conservation and Dynamics

	homeomorphic	heteromorphic
synchronous	rotation of a rigid propeller	stereoisomerization of a molecular propeller[a]
asynchronous	rotation of a supramolecular propeller	stereoisomerization of supramolecular propeller

[a]Suggested mechanism.

area, $X = 2$), which is in agreement with the observations in Figure 2j–m. This morphology lasts for more than 1 ns in the MD simulations at 450 K. During this time the chiral $\Pi(\lambda)$ structure can (i) rearrange homeomorphically (i.e., remaining in the same topology) to its mirror $\Pi(\delta)$ image (E in Figure 5a) or (ii) decay back to the λ propeller (in trajectories not shown). For (i), when the stereoisomerized $\Pi(\delta)$ breaks apart (F in Figure 5) the resulting propeller configuration also has the δ handedness (H in Figure 5).

Table 1 summarizes the previous observations. It is interesting to note that the propeller ($X = 0$) cannot stereoisomerize in two dimensions without changing its topology, which is in contrast with the Π configuration ($X = 2$). These findings might further motivate mathematical studies on topological stereoisomerization in two dimensions. For the second (ii) point, it is worth noting that in 6 out of 18 1-μs-long stereoisomerization trajectories, the $\Pi(\lambda)$ configuration itself can also decay to a propeller structure of the δ enantiomer. However, such mechanism requires the lower Π-foot molecule to detach from the Π-roof molecule, in a manner shown by the red marking in D, Figure 5. Because we have given experimental evidence in Figure 2 that our model favors lateral repulsions between sexiphenyl moieties, this alternative stereoisomerization mechanism seems slightly overestimated by the employed model.

In conclusion, our combined investigation explores mechanistic aspects of supramolecular rotation, revealing asynchronous pathways in a two-step (i.e., nonconcerted) process for caged dynamers. Experimentally, however, rotation appears fully concerted since intermediates are too short-lived to be observed. During rotation, elements of the dynamer rearrange to an intermediate state while conserving topology, followed by crossing of a dominant rate-limiting barrier. Such homeomorphic rotation is asymmetric, whereby during clockwise and anticlockwise rotation the population of intermediate states follows a different sequence. Importantly, the asynchronous crossing of transition barriers from poorly symmetric intermediates lowers the overall rotation barrier compared to synchronous rotation by symmetric intermediates, defining a type of mechanical cooperativity. Further, we revealed that distinct changes in the dynamer topology, that is, heteromorphism, mediates two-dimensional stereoisomerization of a $X = 2$ topology, in marked contrast to homeomorphic rotation. These insights highlight the importance of designing adaptive configurations with weakly connected molecular units, rather than all-rigid architectures in the future synthesis, assembly, and functional integration of man-made molecular machinery. In the biological fields, these studies indicate a potential role of asynchronous topologically conserving pathways as entropically favored mechanisms during molecular motion. Finally, our observations demonstrate the power of dynamic atomistic simulations and nanoscopic measurements for providing new concepts and engineering protocols in molecular science.

■ ASSOCIATED CONTENT

Supporting Information

Experimental Procedures, additional MD trajectories, and detail of network's qualitative free energy analysis. MD movies and MD scripts for rendering the TAPs and external energy per molecule are provided. This material is available free of charge via the Internet at http://pubs.acs.org.

■ AUTHOR INFORMATION

Corresponding Authors

*E-mail: c.a.palma@tum.de (C.-A.P.).
*E-mail: jvb@tum.de (J.V.B.).

Notes

The authors declare no competing financial interest.

■ ACKNOWLEDGMENTS

Work supported by the European Research Council via Advanced Grant MolArt (Grant 247299). J.B. acknowledges the Swedish Research Council for funding and Sven Stafström for support. All authors warmly thank Mario Ruben and Svetlana Klyatskaya for providing the molecules used in the

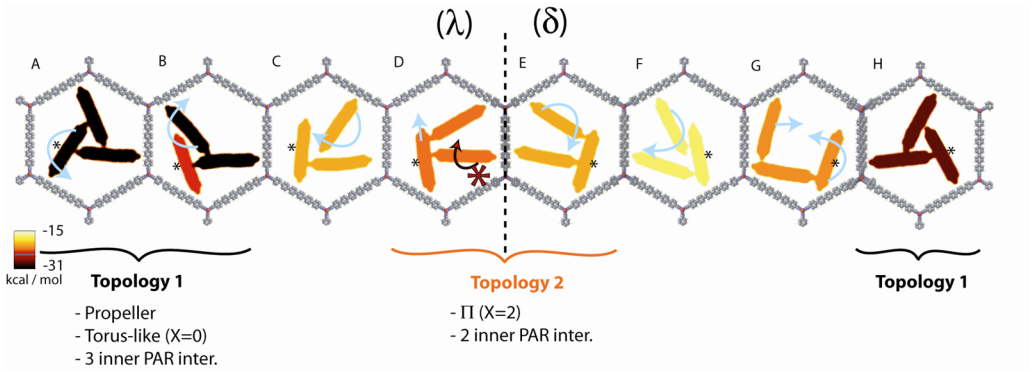

Figure 5. Two-dimensional heteromorphic pathways in the stereoisomerization of a dynamer. Rendered snapshots in a MD trajectory at 450 K. Cyan arrows are used to indicate the next movement in the series. An asterisk is used to guide the eye during rotation. Structures D and E show the "Π" state observed in Figure 2 with a markedly different topology than the propeller configuration. The red asterisk and arrow in structure D indicate an alternative path in the "Π" decay for stereoisomerization of the propeller structure. Note that the energies shown are not comparable to those in Figure 3 because of the use of a restraining 2D potential at 3.0 Å in these simulations.

dx.doi.org/10.1021/nl5014162 | Nano Lett. 2014, 14, 4461–4468

experiments and David Duncan for additional comments. We thank the Swedish National Supercomputing Center project SNIC 001/12-83 for allocated supercomputing resources.

REFERENCES

(1) Koga, N.; Tatsumi-Koga, R.; Liu, G. H.; Xiao, R.; Acton, T. B.; Montelione, G. T.; Baker, D. *Nature* **2012**, *491* (7423), 222−227.
(2) Zhao, G. P.; Perilla, J. R.; Yufenyuy, E. L.; Meng, X.; Chen, B.; Ning, J. Y.; Ahn, J.; Gronenborn, A. M.; Schulten, K.; Aiken, C.; Zhang, P. J. *Nature* **2013**, *497* (7451), 643−646.
(3) Nobel Prize in Chemistry 2013 to Martin Karplus, Michael Levitt, and Arieh Warshel "for the development of multiscale models for complex chemical systems". Nobelprize.org. Nobel Media AB 2014. http://www.nobelprize.org/nobel_prizes/chemistry/laureates/2013/ (accessed July 29, 2014).
(4) Schliwa, M.; Woehlke, G. *Nature* **2003**, *422* (6933), 759−765.
(5) Calimet, N.; Simoes, M.; Changeux, J. P.; Karplus, M.; Taly, A.; Cecchini, M. *Proc. Natl. Acad. Sci. U.S.A.* **2013**, *110* (42), E3987−E3996.
(6) Arai, S.; Saijo, S.; Suzuki, K.; Mizutani, K.; Kakinuma, Y.; Ishizuka-Katsura, Y.; Ohsawa, N.; Terada, T.; Shirouzu, M.; Yokoyama, S.; Iwata, S.; Yamato, I.; Murata, T. *Nature* **2013**, *493*, 703−707.
(7) DeWitt, M. A.; Chang, A. Y.; Combs, P. A.; Yildiz, A. *Science* **2012**, *335* (6065), 221−225.
(8) Lehn, J. M. *Angew. Chem., Int. Ed.* **2013**, *52* (10), 2836−2850.
(9) Akimov, A. V.; Nemukhin, A. V.; Moskovsky, A. A.; Kolomeisky, A. B.; Tour, J. M. *J. Chem. Theor. Comp.* **2008**, *4* (4), 652−656.
(10) Vacek, J.; Michl, J. *Adv. Funct. Mater.* **2007**, *17* (5), 730−739.
(11) Palma, C. A.; Cecchini, M.; Samorì, P. *Chem. Soc. Rev.* **2012**, *41* (10), 3713−3730.
(12) Reimann, P. *Phys. Rep.* **2002**, *361* (2−4), 57−265.
(13) Balzani, V.; Gomez-Lopez, M.; Stoddart, J. F. *Acc. Chem. Res.* **1998**, *31* (7), 405−414.
(14) Sauvage, J. P. *Acc. Chem. Res.* **1998**, *31* (10), 611−619.
(15) Koumura, N.; Zijlstra, R. W. J.; van Delden, R. A.; Harada, N.; Feringa, B. L. *Nature* **1999**, *401* (6749), 152−155.
(16) Leigh, D. A.; Wong, J. K. Y.; Dehez, F.; Zerbetto, F. *Nature* **2003**, *424* (6945), 174−179.
(17) Jewell, A. D.; Tierney, H. L.; Baber, A. E.; Iski, E. V.; Laha, M. M.; Sykes, E. C. H. *J. Phys.: Condens. Matter* **2010**, *22*, 264006.
(18) Lensen, D.; Elemans, J. A. A. W. *Soft Matter* **2012**, *8* (35), 9053−9063.
(19) Gimzewski, J. K.; Joachim, C.; Schlittler, R. R.; Langlais, V.; Tang, H.; Johannsen, I. *Science* **1998**, *281* (5376), 531−533.
(20) Perera, U. G. E.; Ample, F.; Kersell, H.; Zhang, Y.; Vives, G.; Echeverria, J.; Grisolia, M.; Rapenne, G.; Joachim, C.; Hla, S. W. *Nat. Nanotechnol.* **2013**, *8* (1), 46−51.
(21) Kudernac, T.; Ruangsupapichat, N.; Parschau, M.; Macia, B.; Katsonis, N.; Harutyunyan, S. R.; Ernst, K. H.; Feringa, B. L. *Nature* **2011**, *479* (7372), 208−211.
(22) van Delden, R. A.; ter Wiel, M. K. J.; Pollard, M. M.; Vicario, J.; Koumura, N.; Feringa, B. L. *Nature* **2005**, *437* (7063), 1337−1340.
(23) Tierney, H. L.; Murphy, C. J.; Jewell, A. D.; Baber, A. E.; Iski, E. V.; Khodaverdian, H. Y.; McGuire, A. F.; Klebanov, N.; Sykes, E. C. H. *Nat. Nanotechnol.* **2011**, *6* (10), 625−629.
(24) Kühne, D.; Klappenberger, F.; Krenner, W.; Klyatskaya, S.; Ruben, M.; Barth, J. V. *Proc. Natl. Acad. Sci. U.S.A.* **2010**, *107* (50), 21332−21336.
(25) Manzano, C.; Soe, W. H.; Wong, H. S.; Ample, F.; Gourdon, A.; Chandrasekhar, N.; Joachim, C. *Nat. Mater.* **2009**, *8* (7), 576−579.
(26) Polanyi, J. C.; Zewail, A. H. *Acc. Chem. Res.* **1995**, *28* (3), 119−132.
(27) Kühne, D.; Klappenberger, F.; Decker, R.; Schlickum, U.; Brune, H.; Klyatskaya, S.; Ruben, M.; Barth, J. V. *J. Am. Chem. Soc.* **2009**, *131* (11), 3881−3883.
(28) Palma, C.-A.; Björk, J.; Kühne, D.; Klappenberger, F.; Stafström, S.; Barth, J. V. arXiv:1407.7255. (accessed July 29, 2014).
(29) Muetterties, E. *J. Am. Chem. Soc.* **1969**, *91* (7), 1636−1643.
(30) Klyatskaya, S.; Klappenberger, F.; Schlickum, U.; Kühne, D.; Marschall, M.; Reichert, J.; Decker, R.; Krenner, W.; Zoppellaro, G.; Brune, H.; Barth, J. V.; Ruben, M. *Adv. Funct. Mater.* **2011**, *21* (7), 1230−1240.
(31) Arras, E.; Seitsonen, A. P.; Klappenberger, F.; Barth, J. V. *Phys. Chem. Chem. Phys.* **2012**, *14* (46), 15995−16001.
(32) The average ground-state energy is calculated using the external energy histogram at 5 K. In ref 28, the D1 ground state is reported as −0.99 eV (−22.8 kcal mol^{-1}). This corresponds the energy of the structures recentered at 3.2 Å, a strategy employed in order to achieve ergodicity. The lower ground state reported in the current work −0.75 eV (−17.3 kcal mol^{-1}) corresponds to the ground-state energy at the unperturbed adsorption height of 3.5 Å.
(33) As explained in methods and ref 28, all vdW interactions except the hydrogen vdW interactions were removed during energy analysis. Without such vdW removal, the vdW interaction, given by Lennard-Jones (LJ) parameters, of a single D1 molecule with the pore is −4.0 eV (−93.2 kcal mol^{-1}). This quantity largely screens the contribution of the electrostatic interactions, just −0.36 eV (−8.3 kcal mol^{-1}) in the ground state. Note that such large vdW interaction energy is typical of the adsorption of a 64-atom molecule on a surface. For example, already in graphene using eq 1 from Björk, J.; et al. *J. Phys. Chem. Lett.* **2010**, *1* (23), 3407−3412 one finds D1 adsorption energies of −3.9 eV (−90 kcal mol^{-1}). Note that hydrogen vdW interactions are kept in order to provide minimal repulsion contributions due to atomic overlap.
(34) Krenner, W.; Klappenberger, F.; Kepcija, N.; Arras, E.; Makoudi, Y.; Kühne, D.; Klyatskaya, S.; Ruben, M.; Barth, J. V. *J. Phys. Chem. C* **2012**, *116* (31), 16421−16429.
(35) In ref 34, PAR interactions were calculated without the substrate. We note that without the substrate parametrization in the current work (i.e., in isolated dimers), we find an overestimated PAR interaction of −0.43 eV (−10 kcal mol^{-1}) between sexiphenyl dicarbonitriles. This translates to the charge parametrization employed here being valid only with the substrate and as a function of the adsorption height (3.5 Å).
(36) McNaught, A. D.; Wilkinson, A. *IUPAC. Compendium of Chemical Terminology*, 2nd ed.; Blackwell Scientific Publications: Oxford, 1997.
(37) Gfeller, D.; De Los Rios, P.; Caflisch, A.; Rao, F. *Proc. Natl. Acad. Sci. U.S.A.* **2007**, *104* (6), 1817−1822.
(38) Rao, F.; Caflisch, A. *J. Mol. Biol.* **2004**, *342* (1), 299−306.
(39) Fruchterman, T. M. J.; Reingold, E. M. *Software: Pract. Exper.* **1991**, *21* (11), 1129−1164.

NOTE ADDED AFTER ASAP PUBLICATION

This paper was published ASAP on July 31, 2014. A new Supporting Information file, containing four movies and a script file, was made available in the version that was re-posted on August 13, 2014.